- A P P E N D I X A -

WAVEGUIDE EXAMPLE

14.1   Example of Waveguide Calculation

In the section 6.5 we showed how we could use waveguide approaches in the relatively simple spherical coordinate system (compared to OS for example) to approximate the sound transmission through an arbitrary waveguide. In order to make this example as lucid as possible we will consider only a single section. Extending the techniques to multiple sections will be readily apparent once we have shown the techniques as they are applied to a single section.

The problem that we will evaluate is one that is both simple and physically realizable. Figure 6-14a shows a drawing of this example. A four inch midrange
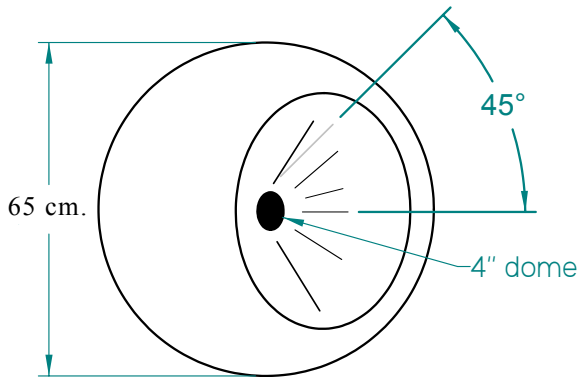
dome with a resonance of 1000 Hz. and a Q of 1.0 is placed at the apex of a spherical horn of 45° - a total 90° encompassed angle. The dome is driven axially so that the input velocity is expressed simply as

$$v_0(\theta) = \cos(\theta)$$

(14.1.1)

owing to the fact that the velocity is not normal to the surface of the dome for points away from its axis. The radius of the dome is assumed to match the radius at the throat of this waveguide, which is then the radius to the throat of the waveguide - 7 cm. The radius to the mouth is chosen to be 33 cm. (about 1 ft.) creating an aperture size of just under 50 cm. in diameter. The enclosure is assumed to be a sphere because of the simplicity of calculating the radiation and

impedance functions. A flat baffle could also be used but would require a few more calculations which would not add anything to the discussion.

The first thing that we must do is to calculate the Eigenvalues and Eigen-functions for a 45° waveguide. By using the shooting method (as described on pg. 138), values for the separation constants λ can be found. After performing this task for several values of angles a pattern began to emerge and the Eigenvalues were found to be predictable from the equation

$$\lambda(m,n) = m^2 n(n+1) = v(v+1) \tag{14.1.2}$$

$$m = \frac{\pi}{2 \cdot angle}$$

$n = 0,2,4...mode\ number$

Only odd values of the mode number are required due to the assumption of axi-symmetry. These values of λ can be seen to be reasonable even though no proof of their validity is evident.

From Eq. (14.1.2) we will then find that,

$$v(m,n) = \frac{\sqrt{1 + 4m^2 n(n+1)} - 1}{2} \tag{14.1.3}$$

which are the eigenvalues for the standard Legendre Eq. 3.4.34. With the eigen-values in hand we can easily generate the angular function using the series solu-tion[1]

$$S_v(\cos(\theta)) = \begin{cases} P_n(\cos(\theta)) & \text{if } v = \text{an integer} \\ \sum_{k=0}^{\text{int}(v)} -1^k \frac{(v+k)!}{k!^2(v-k)!} \left[\frac{(1-x)}{2}\right]^2 - \frac{\sin(v\pi)}{\pi} \sum_{k=\text{int}(v)+1}^{2\text{int}(v)} \frac{(v+k)!(v-k-1)!}{k!^2} \left[\frac{(1-x)}{2}\right]^2 \end{cases} \tag{14.1.4}$$

This series converges very rapidly in the region that we are interested in, i.e. small $(1-x)$.

Fig. 14-1 shows the first five angular modes, although, as we will see, we will only need to use the first three terms for the current problem. Therefor in our problem $m=4$, and $n=0,2,4$. The zero order Eigen-function is unity, which is identical to the normal Legendre function indicating that the zeroth order mode is the same regardless of the angle of the waveguide. This means that if we are only concerned with low frequencies we need only consider this first mode. This is exactly the situation we refered to on pg.131 when we talked about the limited applicability of Websters Equation.

The next step is to calculate the radial functions. This appear, at first, not to be too difficult since we know the eigenvalues. The problems come from stability of

---

1. See Zhang, *Computations of Special Functions*

$S_n(x)$
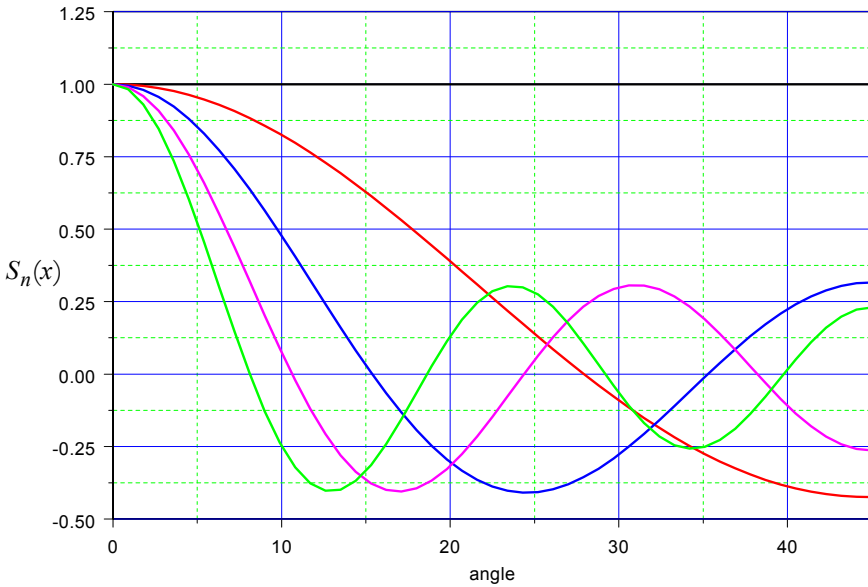
Figure 14-1 - The angular wave functions for 45°

the calculations. By using the well know series solution for Bessel's equation (of arbitray order) we can calculate the radial functions for any value of *m* and *n*.

Fig. 14-1 shows the lowest order radial function as real and imaginary parts along with the derivatives of these functions. All four of these functions will be required for an analysis. The real part of the radial function of the first kind is easy to calculate and converges very rapidly. It also has a well know value at high *kr* which is the same as the normal spherical Hankel functions (see Eq. 3.4.33 on pg. 50). The series solution goes unstable at high *kr* but can be augmented by resorting to the solutions for large arguments allowing the functions to be evaluated anywhere. This melding of solutions will raise its ugly head later in this analysis.

Fig. 14-3 and Fig. 14-4 show the functions for $n=2$ and 4 respectively. Of note in these figures is the obvious "cut-in" phenomena at about $kr=5$ for the $n=2$ mode and $kr=10$ for the $n=4$ mode.

Looking back now to pg. 149 we should point out a few things. First the modes in Eq. (6.5.13) are uncoupled. By this we mean that we can calculate each mode propagation through the waveguide section independent of the other modes, they do not interact. Of course there is always modal interaction and transfer from lower modes to higher modes at each junction of the sections when multiple sections are used (as we discussed in Sec. 6.5), but since we will be dealing with only one section in this example we need not be concerned with modal transfer at the interfaces.

Consider then the T-matrix for an arbitrary mode

n = 0
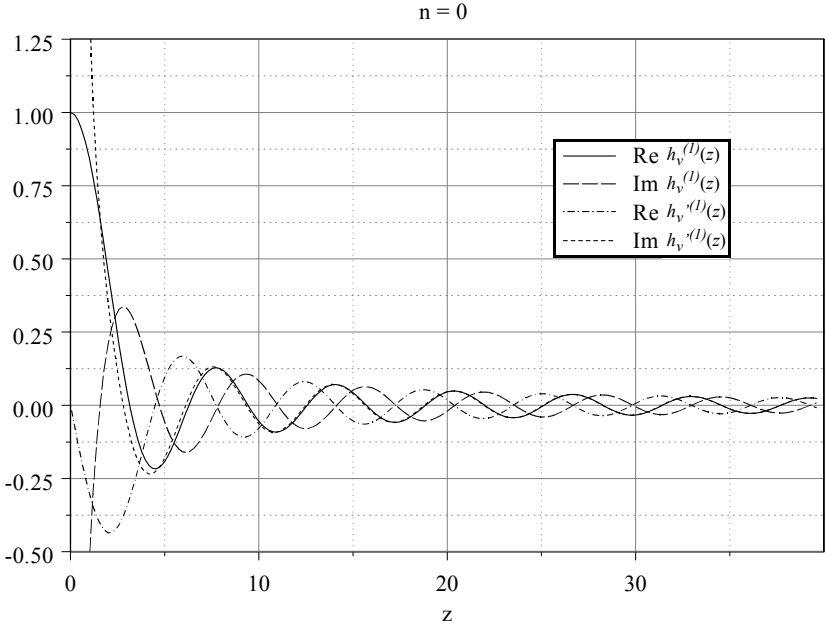
Figure 14-2 - Radial wave functions for 45° waveguide of order zero.

n = 2
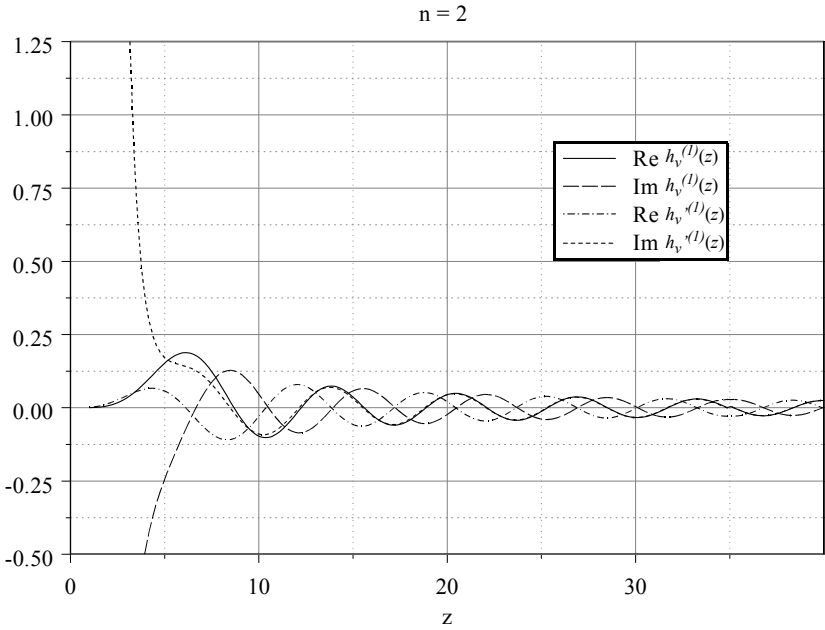
Figure 14-3 - Radial wave functions for 45° waveguide of order two.
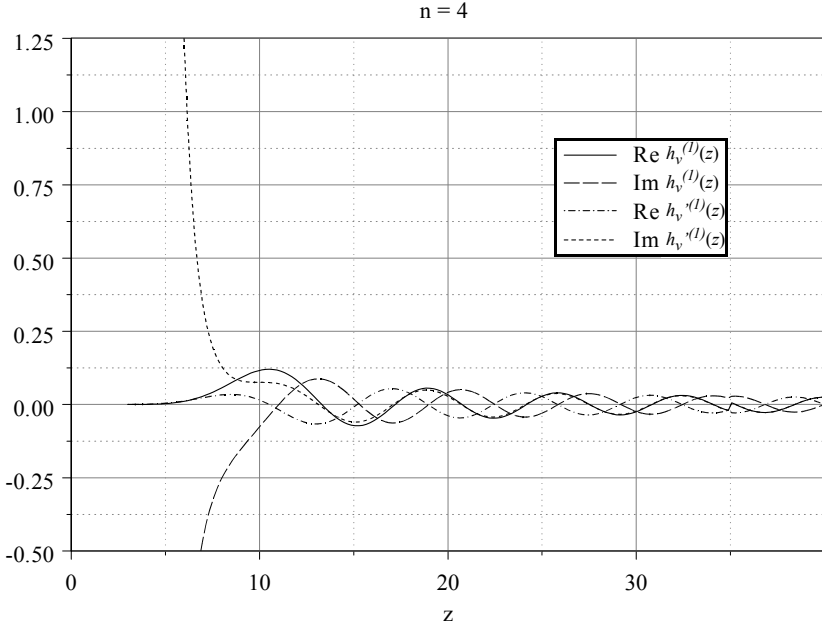
Figure 14-4 - *Radial wave functions for 45° waveguide of order two.*

$$\begin{bmatrix} p_i^v \\ v_i^v \end{bmatrix} = \begin{bmatrix} H_{0,0} & H_{0,1} \\ H_{1,0} & H_{1,1} \end{bmatrix} \begin{bmatrix} p_o^v \\ v_o^v \end{bmatrix} \tag{14.1.5}$$

multiplying this matrix out results in

$$p_i = H_{0,0}(kr)p_o + H_{0,1}(kr)v_o = \left(H_{0,0}(kr)z_o(ka) + H_{0,1}(kr) \right)v_o$$

$$v_i = H_{1,0}(kr)p_o + H_{1,1}(kr)v_o = \left(H_{1,0}(kr)z_o(ka) + H_{1,1}(kr) \right)v_o \tag{14.1.6}$$

   $z_o(ka) =$*specific acoustic impedance at the mouth of radius a*

From these two equations several important relationships can be derived. First, if we divide the upper one by the lower one we will get an expression for the acoustical impedance load on the diaphragm. For brevity we will assume that this impedance has only a negligable effect on the diaphragm motion, which is only slightly eroneous in this case. Next, the second equation can be solved for the velocity v_0 at the mouth for a given velocity v_i at the throat. It is this second function that we are most interested in.

$$v_o(k) = \frac{v_i(k)}{H_{1,0}(k,r_i,r_o)z_0(ka)\rho c + H_{1,1}(k,r_i,r_o)} \frac{S_o}{S_i} \tag{14.1.7}$$

   $S_o =$*area of the mouth*

   $S_i = $ *area of the throat = area of the driver*

where the *H*'s are given by Eq.(6.5.14) (see errata).

A plot of this function is shown in Fig. 14-5. There are only two modal curves
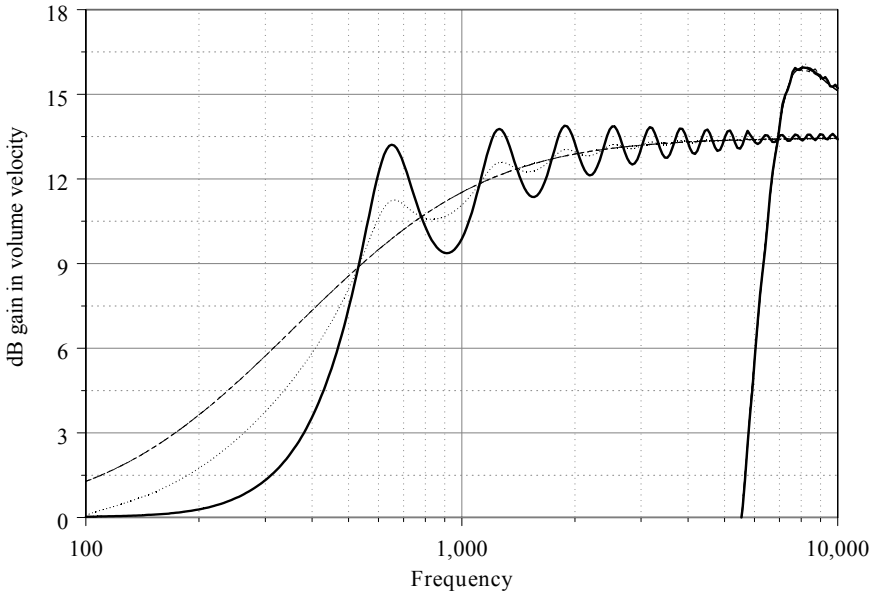
Figure 14-5 - Volume velocity gain resulting from the waveguide.

in this figure since the $n=4$ mode does not come into play below 10kHz. Also shown in this figure as dashed lines are the transfer functions for the $n=0,2$ modes for a completely non-reflecting mouth.

The lowest mode is dominate up until about 7kHz at which point the second mode cuts in and dominates the situation. The volume velocity transfer is unity at low frequencies, as it must be, but there is a substantial increase in the volume velocity above about 700Hz. reaching about 13.5 dB of passband gain. The ripples in the response are related to waves reflected from the mouth and can be reduced by a radius'd (flared) mouth treatment as we discussed in Sec. 6.6. A flared mouth would have a velocity transfer function that lies somewhere between the two curves, reflecting and non-reflecting, as shown by the dotted line in Fig. 14-5.

We are now in a position to calculate the actual wave propagation down the waveguide. To do this we must first expand the throat velocity contour into the wavefunctions for the 45° waveguide - Fig. 14-1. We do this with the following equation,

$$A_n = \int_{x_0}^{1} x \, S_n(x) \, dx \tag{14.1.8}$$

$x = \cos(\theta)$

$x_0 = \cos(\theta_0)$

we must also calculate the normalization

$$\Lambda_n = \int_{x_0}^{1} S_n^2(x) \, dx \tag{14.1.9}$$

Fig. 14-6 shows a plot of the recontructed velocity profile from the first two modes which shows a fairly good match. The higher modes required for a better fit would not propagate down the waveguide so we need not be concerned with fitting this profile any closer than shown in the figure.
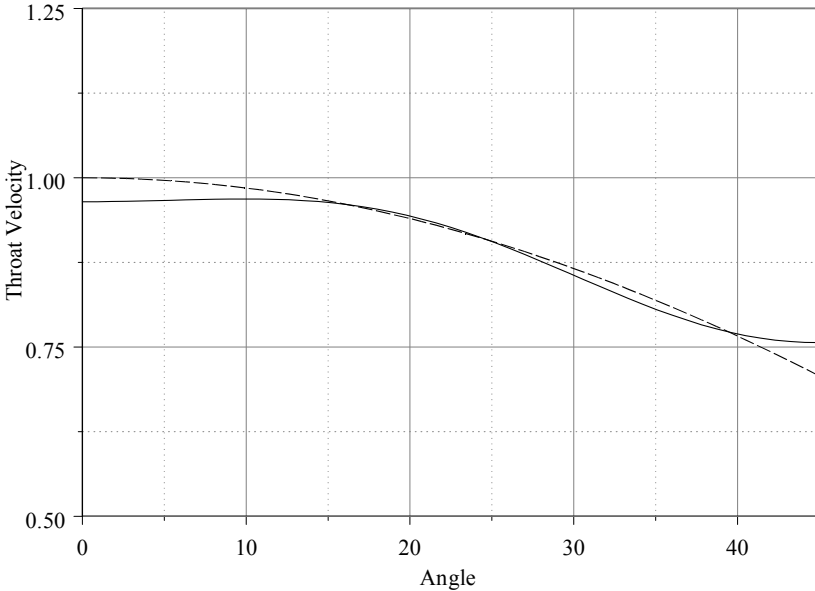
Figure 14-6 - Fitted throat velocity solid - exact dashed

We now use Eq. (14.1.7) to find the velocities at the mouth for each mode and then resum the modes together. The result of this process is shown in Fig. 14-7. This is an interesting result. Below about 6 kHz. there is basically very little change in the mouth velocity - but note that it is radial in nature even though the source vibrated axially. Basically the axial throat velocity has been converted into a spherical wavefront by the nature of the waveguide, because only the n=0, the spherical mode, can propagate at these frequencies. Starting at about 6 kHz. the wavefront is becoming effected by the second mode. This mode causes the wave-
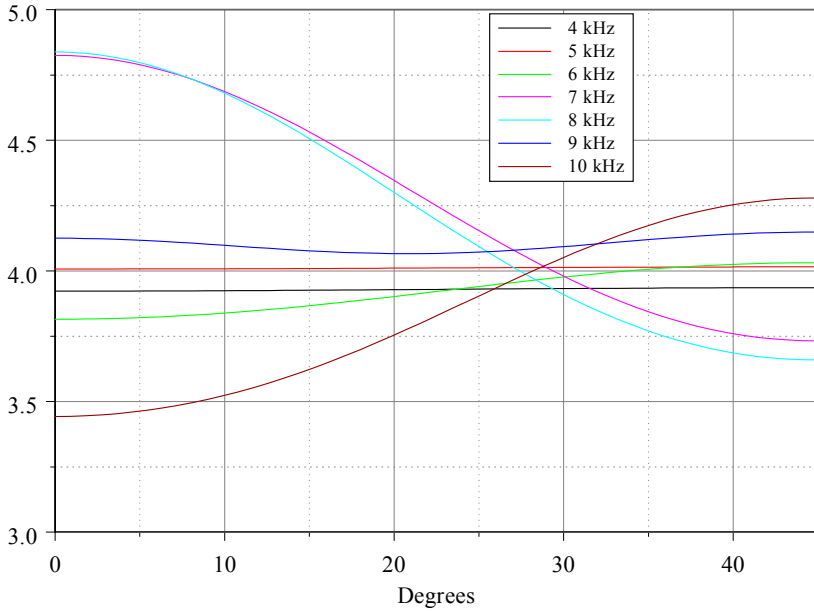
Figure 14-7 - Mouth velocities at various frequencies.

front to be focused into the center of the mouth until at about 10 kHz this effect completely reverses itself. This effect results from a phase change in the second mode, which goes from adding in phase to adding out of phase.

We want to know how this driver waveguide combination will radiate into space. By using the mouth velocities from Fig. 14-7 we can use Eq. (6.6.21) to calculate the radiation map for the device under consideration. We will asume that the mouth is flared into the sphere to reduce diffraction at this junction. The response is shown in Fig. 14-8. and the axial respons is shown in Fig. 14-9.

Figure 14-8 - Polar map for 45° waveguide on a midrange dome.

Figure 14-9 - Axial response of 45° waveguide on a midrange dome